JGR Oceans

RESEARCH ARTICLE
10.1029/2021JC017565

Atmospheric Wind Biases: A Challenge for Simulating the Arctic Ocean in Coupled Models?

C. Hinrichs[1], Q. Wang[1,2], N. Koldunov[1], L. Mu[3], T. Semmler[1], D. Sidorenko[1], and T. Jung[1]

[1]Alfred Wegener Institute Helmholtz Center for Polar and Marine Research, Bremerhaven, Germany, [2]Laboratory for Regional Oceanography and Numerical Modeling, Pilot National Laboratory for Marine Science and Technology, Qingdao, China, [3]Pilot National Laboratory for Marine Science and Technology, Qingdao, China

Abstract Many state-of-the-art climate models do not simulate the Atlantic Water (AW) layer in the Arctic Ocean realistically enough to address the question of future Arctic Atlantification and its associated feedback. Biases concerning the AW layer are commonly related to insufficient resolution and excessive mixing in the ocean component as well as unrealistic Atlantic-Arctic Ocean exchange. Based on sensitivity experiments with FESOM1.4, the ocean–sea-ice component of the global climate model AWI-CM1, we show that even if all impediments for simulating AW realistically are addressed in the ocean model, new biases in the AW layer develop after coupling to an atmosphere model. By replacing the wind forcing over the Arctic with winds from a coupled simulation we show that a common bias in the atmospheric sea level pressure (SLP) gradient and its associated wind bias lead to differences in surface stress and Ekman transport. Fresh surface water gets redistributed leading to changes in halosteric height distribution. Those changes lead to strengthening of the anticyclonic surface circulation in the Canadian Basin, so that the deep counterflow carrying warm AW gets reversed and a warm bias in the Canadian Basin develops. The SLP and anticyclonic wind bias in the Nordic Seas weaken the cyclonic circulation leading to reduced AW transport into the Arctic Ocean through Fram Strait but increased AW transport through the Barents Sea Opening. These effects together lead to a cold bias in the Eurasian Basin. An underestimation of sea ice concentration can significantly amplify the induced ocean biases.

Plain Language Summary Coupled global climate models are used to predict anthropogenic climate change along with its impacts. The Arctic has experienced amplified warming in the recent decades compared to global mean warming and therefore is one region of intense climate research. In this context Atlantification of the Arctic Ocean has become a high priority topic. Atlantification describes the increasing impact of oceanic heat from the Atlantic Water (AW) layer of the Arctic Ocean on the sea ice cover. In climate models, the direction and strength of simulated AW circulation around the Arctic Ocean is known to be sensitive to ocean grid resolution, parametrization, boundary and surface forcing or a combination thereof. Here we show that biases in the atmospheric component of climate models can interrupt and even reverse the simulated AW circulation at depth. Such biases can be further amplified by a negative bias in simulated sea ice cover. This study shows how these surface biases can negatively impact the deep ocean circulation.

Key Points:

- Many state-of-the-art climate models fail to simulate the properties of the Atlantic Water layer in the Arctic Ocean realistically
- Biases in Arctic sea level pressure and surface winds in atmosphere models can reverse Atlantic Water circulation
- The underestimation of sea-ice cover amplifies this problem further

Supporting Information:

Supporting Information may be found in the online version of this article.

Correspondence to:

C. Hinrichs,
Claudia.Hinrichs@awi.de

Citation:

Hinrichs, C., Wang, Q., Koldunov, N., Mu, L., Semmler, T., Sidorenko, D., & Jung, T. (2021). Atmospheric wind biases: A challenge for simulating the Arctic Ocean in coupled models? *Journal of Geophysical Research: Oceans*, *126*, e2021JC017565. https://doi.org/10.1029/2021JC017565

Received 10 MAY 2021
Accepted 5 OCT 2021

1. Introduction

The Arctic is one of the fastest changing regions in the world (Serreze & Barry, 2011; Serreze et al., 2009) and hence it has attracted an increasing amount of scientists' attention. Global climate models are used to predict changes in the climate system, including the Arctic, in a warming world, and to understand climate dynamics and associated feedback. Efforts are ongoing to improve the representation of key processes in contemporary climate models, both in general and specifically in the Arctic. The ultimate aim is to increase predictive capacity (Jung et al., 2016). Of particular interest is the process of oceanic heat transport from the North Atlantic into the Arctic Ocean in the form of Atlantic Water (AW) inflow and subsequent AW circulation and heat distribution within the Arctic Basin and how it will change in the future.

A warming trend in the AW layer has been observed at Fram Strait and in the Arctic Ocean over the last few decades (Beszczynska-Möller et al., 2012; Dmitrenko et al., 2008; Polyakov et al., 2005, 2013). This

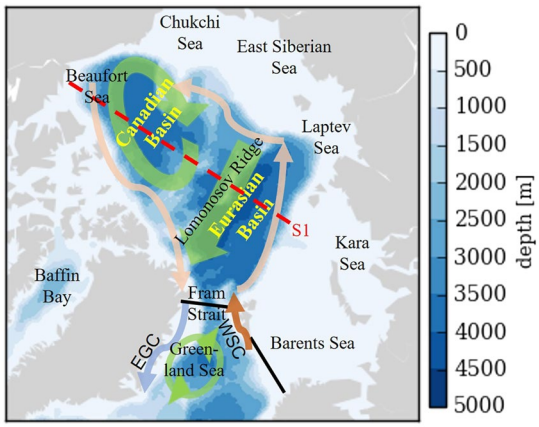

Figure 1. Map of the Arctic Ocean. Depicted are the two deep basins (Canadian and Eurasian Basin) divided by the Lomonosov Ridge, the shelf seas and neighboring seas. A schematic view of the dominant features of Arctic Ocean circulation shows the anticyclonic Beaufort Gyre System, the Transpolar Drift Stream (in green) and the subsurface cyclonic flow of AW around the Arctic Basin (in pink); south of Fram Strait, the Greenland Sea Gyre (GSG; in green); and the West Spitsbergen Current (WSC, orange) and the East Greenland Current (EGC, light blue). Sections where transports through Fram Strait and the southern Barents Sea Opening are computed are shown in black. The dashed red line (S1) shows a section along 130°W/70°E across the deep Arctic Ocean.

warming trend of the AW layer, together with weaker stratification in the upper ocean, has been termed *Atlantification* by Polyakov et al. (2017). Atlantification has been identified as critical to a warming Arctic. In both the Barents Sea and the Eurasian Basin (EB), Atlantification leads to increased bottom-melt of sea ice, weakened stratification, increased surface temperatures and lower albedo (Barton et al., 2018; Ivanov et al., 2018; Koenigk & Brodeau, 2014; Polyakov et al., 2017, 2020).

Both oceanic and atmospheric forcing can contribute to Arctic Atlantification (Asbjørnsen et al., 2020; Shu et al., 2021). Positive temperature trends have been observed in the AW inflow regions in both Fram Strait (Beszczynska-Möller et al., 2012; Onarheim et al., 2014; Wang et al., 2020) and the Barents Sea in recent decades (Boitsov et al., 2012; Wang et al., 2019). Studies show that temperature and salinity anomalies can originate in the Atlantic Subpolar Gyre and travel through the Nordic Seas to the Arctic Ocean (Årthun & Eldevik, 2016; Hátún et al., 2005; Holliday et al., 2008); alternatively, they can be generated locally, within the Nordic Seas, and then travel poleward (Chatterjee et al., 2018; Furevik, 2001). These warm anomalies can cause basal melting of sea ice in the Arctic Ocean. Local atmospheric forcing is also a very important factor in sea-ice decline (Olonscheck et al., 2019). The decrease in sea ice and associated feedback contribute to amplified climate change in the Arctic, which in turn affects the AW layer in the Arctic Ocean. A model study by Itkin et al. (2014) suggests, for example, that thinner, more mobile sea ice in the central Arctic weakens the cyclonic circulation of AW. Another study, by Wang et al. (2020), shows that the Arctic sea-ice decline has strengthened AW heat influx through Fram Strait in the early 21st century through impacts on ocean circulation in the Nordic Seas. There is also an ongoing debate over whether and to what degree Arctic changes, especially changes in sea-ice cover in the Barents Sea, might influence the climate and ocean at lower latitudes (Cohen et al., 2020; Vihma, 2014; Wallace et al., 2014).

An important tool to understand and predict the evolution of this complex system are coupled climate models constrained by observations. However, the degree to which we can trust climate-model predictions of the role of Atlantification in Arctic climate change hinges on the given model's ability to realistically simulate present-day AW inflow and circulation within the Arctic Ocean.

Circulation in the Arctic Ocean can be described as a two-layered system (e.g., Aagaard, 1989; for a recent comprehensive review of Arctic Ocean circulation dynamics, see Timmermans & Marshall, 2020). The large-scale ocean-surface circulation is anticyclonic and driven by the dominating wind systems centered over the Beaufort Gyre and the Transpolar Drift Zone. Below the surface layer, the flow at intermediate depths is largely confined to narrow boundary currents along the steep slopes of the Eurasian and Canadian Basins (see Figure 1). These boundary currents form a cyclonic flow around the deep Arctic Basin in the opposite direction of the upper-ocean drift. Relatively warm, salty AW circulates around the Arctic in this cyclonic boundary current (Karcher et al., 2007; Rudels et al., 1999; Spall, 2013; Woodgate et al., 2001) at a mean depth of around 400 m. The strength and direction of this Arctic circumpolar boundary current (ACBC) determines the spatial distribution and storage of heat in the Arctic Ocean at this intermediate depth.

With this in mind, we compared Arctic Ocean temperatures in the Alfred Wegener Institute coupled climate model AWI-CM1 (Rackow et al., 2016; Semmler et al., 2020; Sidorenko et al., 2015) to the PHC3.0 climatology (Steele et al., 2001) at 400 m depth (Figures 2a and 2b) as well as the mean vertical temperature profiles in both deep basins (Figures 2c and 2d). The temperature maxima in each profile indicate the location of warm AW in the water column. Generally, the vertical temperature profiles averaged over the Eurasian and Canadian basins show that AWI-CM1 and the observational climatology are in good agreement except for in the Eurasian Basin, in the AW layer between 200 and 600 m depths, where AWI-CM1 exhibits a cold bias. But the basin-average temperature profiles do not yield any information about the spatial distribution and

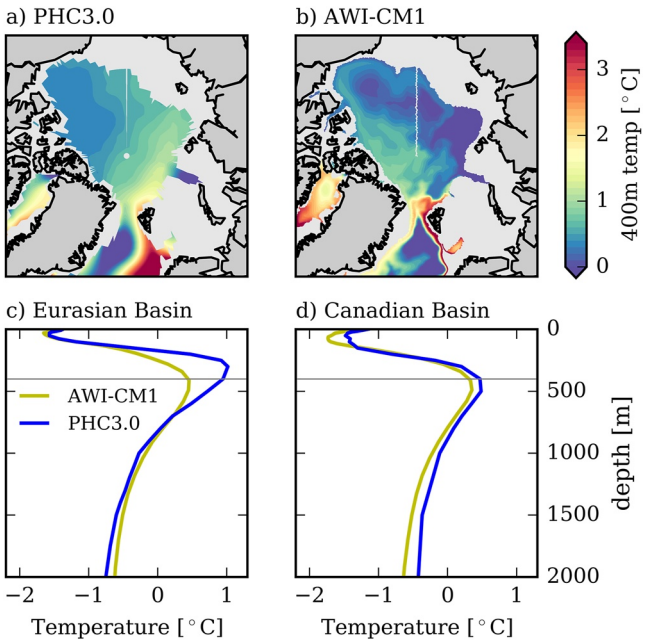

Figure 2. Horizontal distribution of potential temperature [°C] at 400 m depth from the PHC3.0 climatology (a) and the mean potential temperature (1980–1989) at 400 m depth from a coupled AWI-CM1 LR historical simulation (b). This LR simulation was run on an ocean grid with 25 km resolution north of 50°N and at T63 atmospheric resolution. A similarly biased temperature pattern is also evident in AWI-CM1 runs with higher oceanic or atmospheric resolution. Mean vertical temperature profiles over the Eurasian Basin (c) and Canadian Basin (d) are shown for the PHC3.0 climatology and the AWI-CM1 LR simulation. The temperature maxima indicate the average core depth of Atlantic Water. The thin gray line indicates the 400 m depth shown in the horizontal sections in (a and b).

presumed direction of AW circulation within each basin. Those characteristics are better visualized in the 400 m horizontal temperature slice (Figures 2a and 2b) that shows the large-scale features and pathways of warm AW in the Arctic basin. In choosing to evaluate the horizontal temperature distribution at 400 m depth, we follow the model evaluation example of the Coordinated Ocean-ice Reference Experiments (CORE-II; Ilıcak et al., 2016). For the AWI-CM1 simulation, comparison with PHC3.0 reveals an unrealistic distribution of AW: Warm AW that enters through Fram Strait does not follow the Arctic's deep basin slope cyclonically but rather gets diverted westward toward the Canadian Basin. The result is a cold bias in the eastern Eurasian Basin and a warm bias in the Canadian Basin, which is reminiscent of an anticyclonic circulation pattern.

It was somewhat surprising to find these respective biases after standalone simulations with AWI-CM1's ocean–sea-ice component FESOM1.4 had shown a very realistic temperature distribution and a cyclonic circumpolar boundary current at horizontal resolutions of 25 and 4.5 km in the Arctic (Wang et al., 2018).

It is worth stressing that AWI-CM1 is not the only model to show deficiencies in simulating the propagation of AW around the Arctic as some recent studies have revealed. Shu et al. (2019), for example, evaluated a number of CMIP5 models and found that 9 out of 41 participating models did not simulate a well-defined AW layer at all. The multi-model mean (MMM) AW layer derived from the other 32 models was too thick and too deep. Furthermore, they found that the interannual variability in AW temperature was much weaker than observed, and none of the models simulated the warming trend observed in the recent decades. A follow-up study of 23 CMIP6 models by Khosravi et al. (2021) shows that the AW layer is still too deep and too thick in most models and the MMM, suggesting that representation of Arctic Ocean hydrography did not visibly improve between CMIP5 and CMIP6. For AWI-CM1, that study shows a simulated average AW core depth for present-day conditions in range with observations; that is, the AW layer is not too deep in AWI-CM1 as it is in many other models. At the same time, the simulated average AW core temperature is lower than observed, and the simulation shows no pronounced warming of the AW for the historical period. Before CMIP6, the problem of incorrect AW simulation was also recognized in standalone ocean models in the CORE-II model intercomparison study (Ilıcak et al., 2016). Suggested solutions for the AW problem have focused on improving the ocean–sea-ice model and include moving to higher-order advection schemes (Holloway et al., 2007; Maqueda & Holloway, 2006), using eddy–topography interaction parameterization ("Neptune parametrization"; Golubeva & Platov, 2007; Holloway & Wang, 2009; Nazarenko et al., 1998), tuning vertical mixing (Zhang & Steele, 2007) and increasing horizontal resolution (Wang et al., 2018). For AWI-CM1, we find that additional challenges may arise when a well-tuned (with respect to AW in the Arctic Ocean) ocean–sea-ice model, here FESOM 1.4, is coupled to an atmospheric model, in this case ECHAM6.3, to form a coupled climate model.

In this paper we aim to understand the processes causing the deterioration of the AW layer in AWI-CM1. If the standalone version of an ocean–sea-ice model can successfully replicate the two-layered circulation in the Arctic Ocean but coupling leads to perturbed AW circulation, then the reason must lie in the changes in ocean-surface forcing after coupling with the atmospheric model. Our investigations narrowed down the potential origins of these biases to a large-scale bias in sea-level pressure and associated wind field as well as a negative bias in sea-ice cover in the coupled model. Both biases had an impact on the surface stress imparted on the ocean. We conducted sensitivity experiments with our standalone ocean–sea-ice model to analyze the influence of biased wind and sea-ice cover over the Arctic.

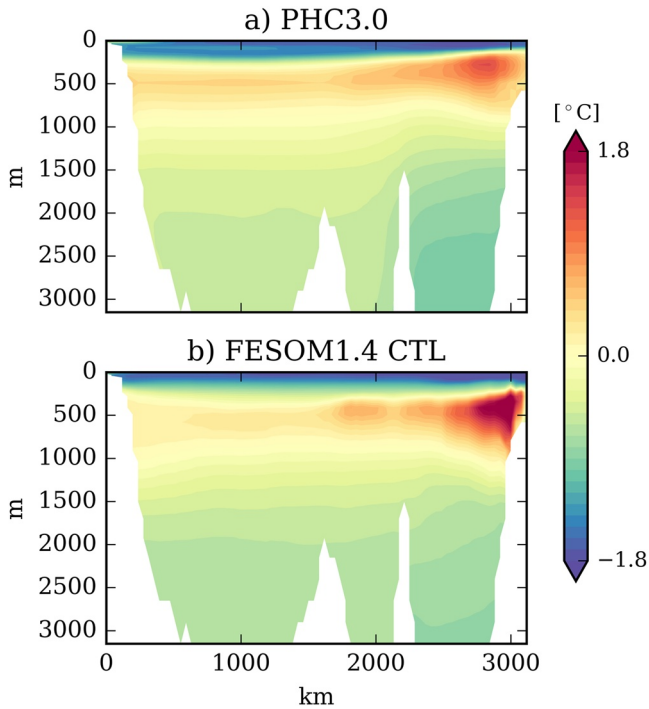

Figure 3. Potential temperature along a section across the deep Arctic Ocean from 130°W/70°N to 70°E/81°N (see section S1 on the map in Figure 1) in the PHC3.0 climatology (a) and mean potential temperature (1980–1989) in a FESOM1.4 simulation with CORE2 forcing (b).

2. Model Set-Up and Sensitivity Experiments

2.1. FESOM1.4 Model Configuration

To study the effect of atmospheric forcing and sea-ice concentration on the AW circulation, we use the **F**inite **E**lement **S**ea ice-Ocean Model FESOM1.4 (Danilov et al., 2015; Wang et al., 2014) in a standalone mode. FESOM1.4 is the ocean–sea-ice component of the AWI-CM1 model, which is FESOM1.4 coupled to ECHAM6.3 (Stevens et al., 2013). The global performance of AWI-CM1 has been evaluated by Sidorenko et al. (2015) and Rackow et al. (2016); the AWI-CM1 contribution to CMIP6 has been evaluated by Semmler et al. (2020). The ocean–sea-ice component, FESOM1.4, employs unstructured grids that allow for increased grid resolution in an area of interest (e.g., the Arctic) while keeping coarser resolution elsewhere. This, along with excellent scalability characteristics (Koldunov et al., 2019), makes longer, global simulations feasible. At least for AWI-CM1, the problem of incorrect AW circulation and distribution in the coupled set-up is mostly independent of ocean and atmosphere resolution. Our experiments are therefore run on the "baseline" ocean grid which was developed for participation in the CORE-II model intercomparison study (Griffies et al., 2009; Ilıcak et al., 2016; Wang et al., 2016a, 2016b). This ocean grid has a global nominal resolution of 1°; however, the resolution has been refined to about 25 km north of 50°N and to 1/3° at the equator as well as moderately along the coasts. The skill of FESOM1.4 at simulating Arctic hydrography with this baseline mesh has been evaluated comprehensively within the CORE-II model intercomparison study (Ilıcak et al., 2016; Wang et al., 2016b) and by Wang et al. (2018). The latter publication assessed the model's skill in comparison to a higher-resolution mesh, including its ability to reproduce the observed warming of the AW layer in the late twentieth century. Both setups–baseline and high-resolution–simulate this observed warming quite well. Although the ocean circulation itself is not directly evaluated in the CORE-II model intercomparison study, the 400 m temperature layer is shown for each model; and for FESOM1.4, the temperature distribution indicates a realistic pathway of AW into and around the Arctic (Ilıcak et al., 2016). Moreover, a more detailed evaluation of Atlantic Water core temperature (AWCT) and Atlantic Water core depth (AWCD) in simulations on this baseline grid show a temperature pattern indicating the correct circulation direction (Wang et al., 2018). Here, we show that this setup reproduces the vertical temperature structure in the Arctic Ocean very well (Figure 3); for more details on the model performance, we would refer the readers to the aforementioned references.

Comparing AWI-CM1 coupled simulations to atmospheric reanalysis data and satellite observations of sea ice revealed biases in the wind field over the Arctic as well as in the sea-ice cover. We presently consider these as possible candidates for causing biases in the ocean in the coupled setup. Accordingly, we ran sensitivity simulations from 1958 to 1989 and compare differences among simulations for the final 10 years from 1980–1989 (see Section 2.3). Therefore, while we show the biases of the coupled model compared to observational and reanalysis products for the period 1980–1989 please note that the biases are similar for other time periods as well (see Figure S1). The following section briefly describes these biases.

2.2. Coupled Model Bias in Mean Sea-Level Pressure and Sea Ice

The comparison of mean sea-level pressure (SLP) to the ERA5 reanalysis data set (Hersbach et al., 2020) shows that AWI-CM1 exhibits a bias over the central Arctic. This bias displays a dipole pattern: erroneously low SLP is found over the Canadian Basin whereas SLP is biased high over the Eurasian Basin and over the Barents and Kara seas (Figure 4). The reduced pressure gradient is associated with a shift of the Beaufort High toward the Eurasian Arctic.

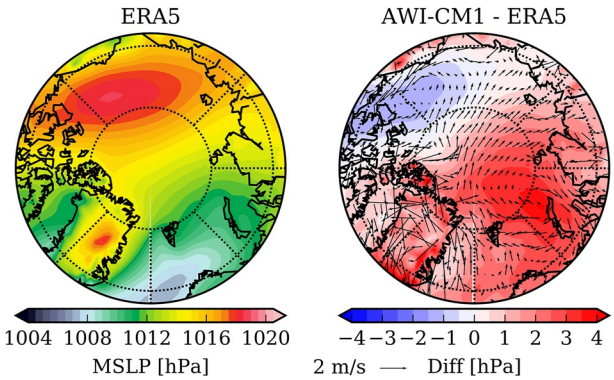

Figure 4. Mean sea-level pressure (MSLP, [hPa]) averaged over 1980–1989 in ERA5 (left) and the MSLP bias [hPa] and associated wind bias in AWI-CM1 (right).

This dipole bias pattern is not unique to AWI-CM1. The coupled climate model MPI-ESM (Müller et al., 2018), which also uses ECHAM6.3 but with a different ocean–sea-ice model, shows the same bias in pattern and magnitude (not shown). A similar SLP bias pattern also dominated the model mean of other atmospheric and coupled models not including ECHAM, and this particular pattern has been attributed to the truncation of the North Atlantic storm track in atmosphere models (Walsh et al., 2002).

When sea-ice concentration from the coupled AWI-CM1 simulation is compared on one hand to the results from the standalone ocean–sea-ice model FESOM1.4 and on the other hand to a gridded sea-ice concentration data product based on satellite observations of brightness temperature provided by the National Snow and Ice Data Center (NSIDC; Cavalieri et al., 1996), it is apparent that AWI-CM1 overestimates sea-ice concentration in the Greenland Sea and eastern Barents Sea in March, when it is at its maximum extent (Figure 5c). This is similar to the results from FESOM1.4 (Figure 5b). In September, when sea-ice extent is at its minimum, AWI-CM1 underestimates the observed minimum sea-ice concentration in the central Arctic and predicts less sea ice than FESOM1.4 forced with CORE-II forcing (Figure 5, bottom row). Only in some shelf regions, including the northeastern Barents Sea and the East Siberian Sea, more sea ice is simulated than observed.

2.3. Sensitivity Experiments

Three sensitivity experiments have been devised to determine the impact of the biases in wind and sea-ice cover (both separately and together) on AW circulation at depth (Table 1). A control simulation and the sensitivity experiments are initialized in 1958 using EN4 climatology (Good et al., 2013) and run with CORE-II forcing (Large & Yeager, 2009) for 32 years, until 1990. In sensitivity experiment 1 (WIND), the 6-hourly CORE-II wind forcing north of 67°N, the Arctic Circle, was replaced with wind from an AWI-CM1 historical

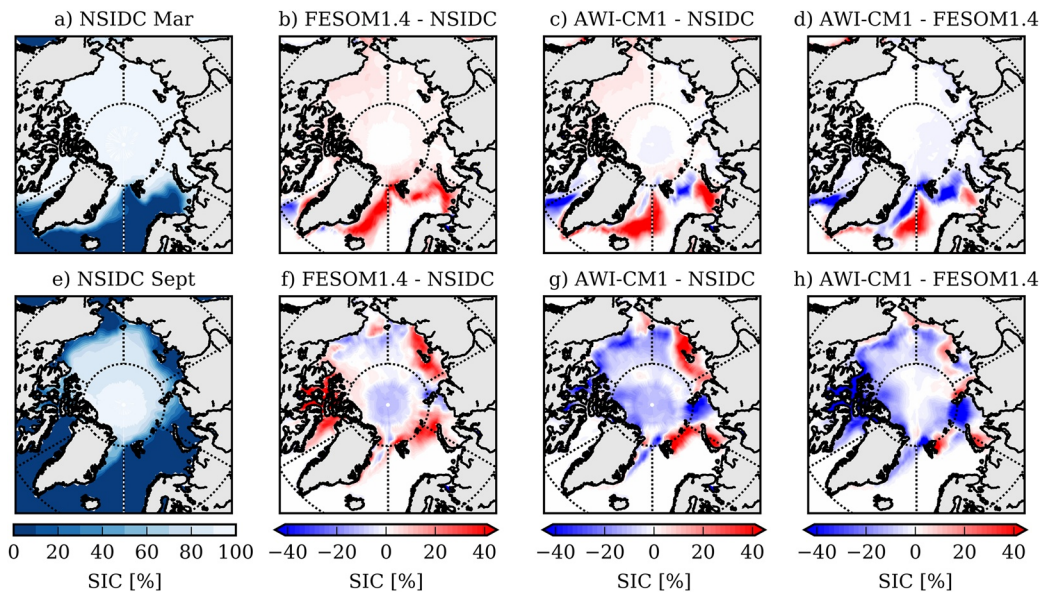

Figure 5. Mean March (a) and September (e) sea-ice concentration (SIC, [%]) from the National Snow and Ice Data Center (NSIDC) for the period 1980–1989, the difference in SIC between FESOM1.4 and NSIDC (b and f), the difference in SIC between AWI-CM1 and NSIDC (c and g), and the difference in SIC between AWI-CM1 and FESOM1.4 (d and h). In March, both FESOM1.4 and AWI-CM1 overestimate SIC in the Greenland Sea and Barents Sea. In September, AWI-CM1 simulates less SIC than observed and less than the standalone model FESOM1.4.

Table 1
Overview of Sensitivity Experiments

	CTL	WIND	ALBEDO	WIND + ALB
Wind Forcing	CORE2 forcing	CORE2 forcing, except wind forcing north of 67°N replaced with wind from coupled simulation	CORE2 forcing	CORE2 forcing, except wind forcing north of 67°N replaced with wind from coupled simulation
Albedo Parameters	default	default	reduced	reduced

simulation run on the same ocean grid, also started in 1958 from EN4. The 6-hourly AWI-CM1 wind output was interpolated onto the CORE-II forcing grid. In sensitivity experiment 2 (ALBEDO), the ice and snow albedos are lowered to such a degree that sea-ice cover is reduced to values similar to the ones found in the coupled simulation. Sensitivity experiment 3 (WIND + ALB) applied both of these changes together. Freshwater forcing is the same for all four experiments, with monthly varying precipitation and monthly climatological continental runoff.

In all four experiments, the drag coefficients for wind-stress computation over ice and water were adapted to track the stress computation in the atmospheric component of AWI-CM1, ECHAM6.3, as closely as possible. The neutral drag coefficient over ice $Cd_{n,i}$ is set to 1.89×10^{-3}, the same value as in ECHAM6.3. The neutral drag coefficient over water $Cd_{n,w}$ is usually dependent on wind speed and is computed using a bulk formula. In ECHAM6.3 it is computed using the Charnock equation (Charnock, 1955). For our experiments using FESOM1.4, the neutral drag coefficient over water $Cd_{n,w}$ was set to a constant value of 1.285×10^{-3} that represents the mean value of applying the Charnock relation to the most common wind-speed values over the Arctic, which are between 1 m/s and 8 m/s.

3. Results of Sensitivity Experiments

First comes the assessment of the effects of changing the wind forcing and lowering the albedo on mean sea-ice concentration in March and September (Figure 6). In winter, replacing the wind forcing over the Arctic Circle with wind from the coupled model results in increased sea-ice concentration along the ice edge in the Greenland Sea and eastern Barents Sea. Spatially more confined reductions in sea-ice concentration can be seen in Davis Strait and in the central Barents Sea. In March, the reduced albedo has almost no effect on sea-ice extent but some effect on sea-ice thickness (not shown). Therefore, the wind replacement governs the combined effect of changed wind forcing and reduced albedo in terms of sea-ice concentration

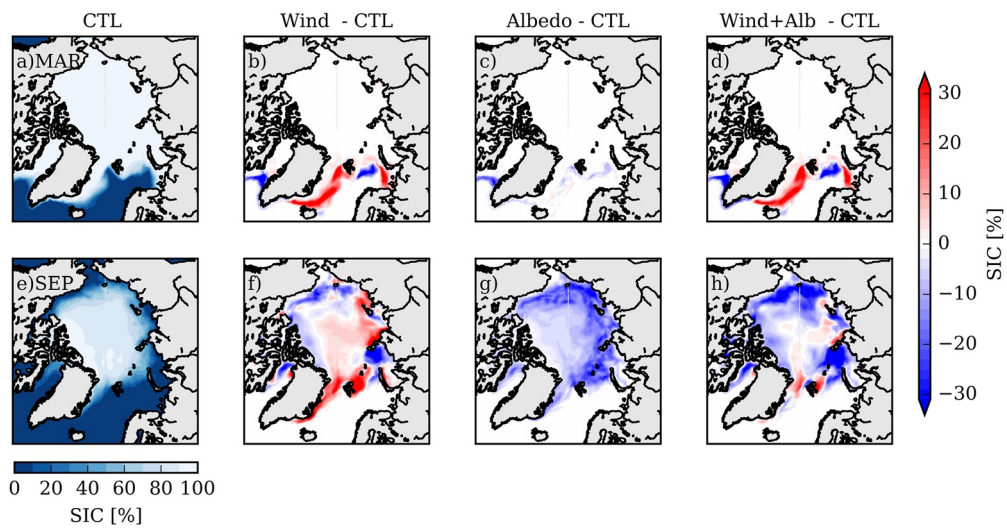

Figure 6. Simulated sea-ice concentration (SIC, [%]) in the control run for March (a) and September (e), and differences in SIC to control run for experiment WIND (b and f), Albedo (c and g) and Wind + Alb (d,h), all averaged over the last 10 years of simulation (1980–1989).

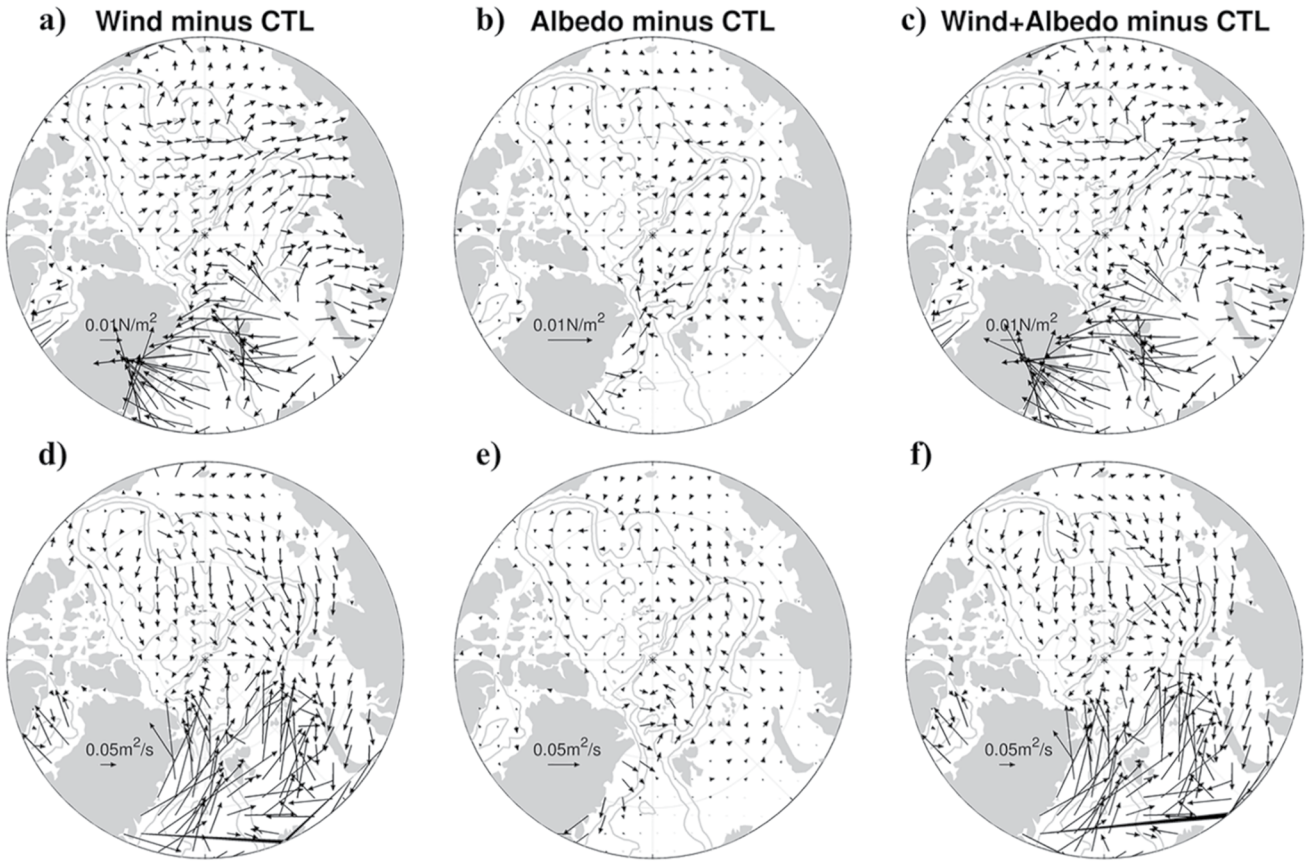

Figure 7. Ocean surface stress difference [N/m^2] (a–c) and Ekman transport difference [m^2/s] (d–f) for the three sensitivity experiments relative to the control run averaged over the last 10 years of simulation (1980–1989). Note that the scale for the experiment ALBEDO is doubled.

in March. The differences in sea-ice concentration between the experiments shown for the month of March (Figures 6a–6d) are representative of each month from November to April, when shortwave radiation is low and sea ice is more compact.

In September (Figures 6e–6h), the wind replacement leads to decreased sea-ice concentration north of the Canadian Archipelago and in the Beaufort, Chukchi, East Siberian and Kara seas but to increased sea-ice concentration in the Laptev Sea, in the central Arctic along the transpolar drift route, in the northern Barents Sea and along eastern Greenland. Reduced albedo leads to a decrease in sea-ice concentration everywhere. In experiment WIND + ALB, which combines wind replacement and albedo reduction, sea-ice concentration is mostly lower than in the control simulation, except along the transpolar drift route and east of Svalbard, which is associated with the impact of winds. The differences for the month of September (Figures 6e–6h) show the maximum effects of the wind replacement and albedo reduction in the melt season, and this is representative of situations from May to October. Mean differences in sea-ice concentration are depicted for each individual month in Figure S2.

Next to be investigated was the effect of the replaced wind and albedo reduction on ocean surface conditions. The difference in surface stress between the sensitivity experiment with replaced wind forcing and the control run in the central Arctic (Figure 7a) is generally acting from the Canadian Arctic Archipelago toward the Siberian side. In the Barents Sea and the Nordic Seas, the difference in surface stress is directed westward. The difference in surface stress due to reduced sea-ice cover is relatively small, showing a westward component in the Eurasian Basin (Figure 7b, note different scale). Differences due to the replaced wind dominate the sensitivity experiment WIND + ALB (Figure 7c).

The differences in surface stress lead to differences in Ekman transport. In the experiments with replaced wind forcing, the transport anomaly in the central Arctic is from the Canadian Basin toward the Eurasian

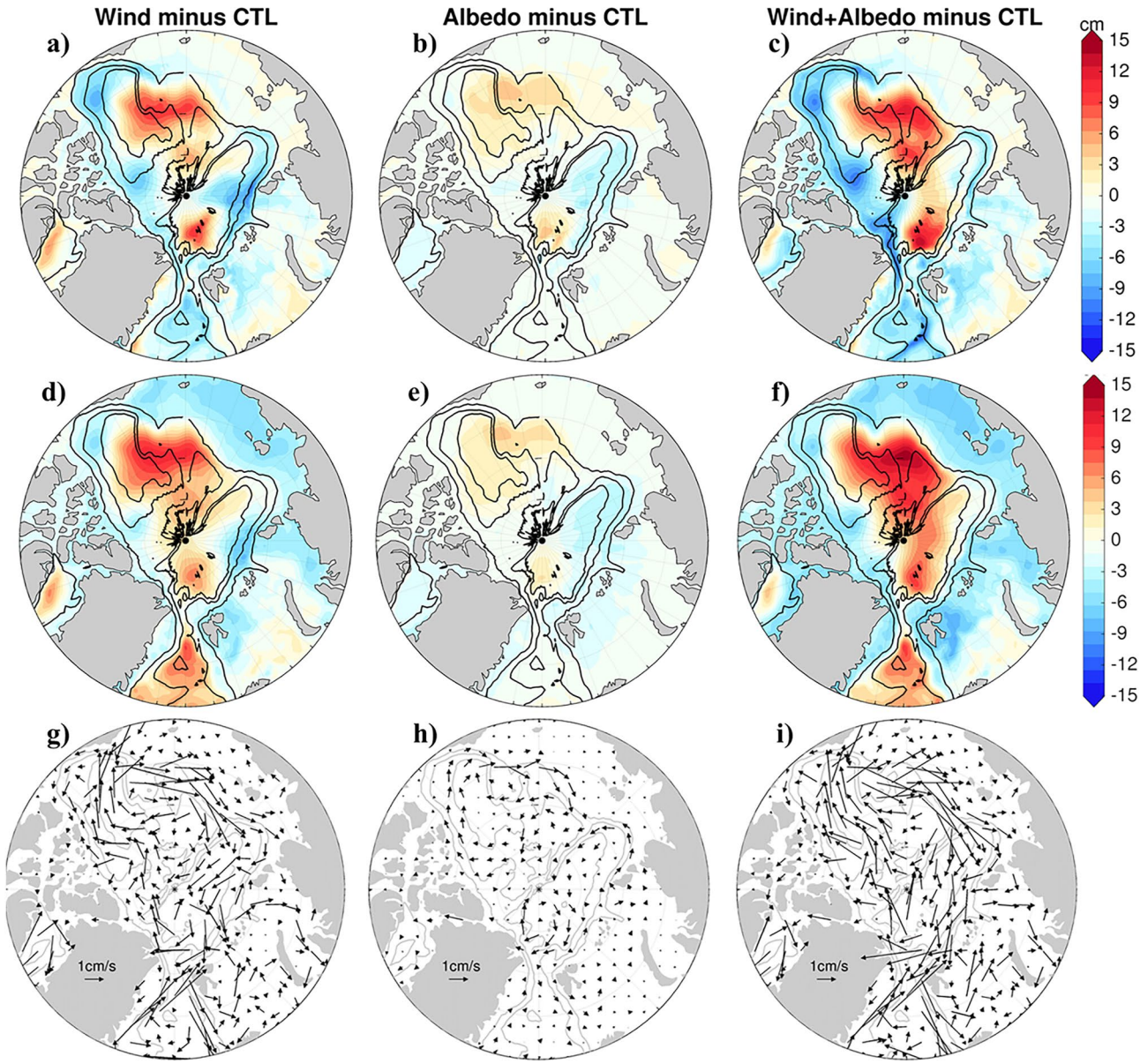

Figure 8. Halosteric height difference [cm] (a–c), sea surface height difference [cm] (d–f) and differences in geostrophic surface current velocity [cm/s] (g–i) for the three sensitivity experiments compared to the control simulation, averaged over the last 10 years of simulation (1980–1989).

side. In the Nordic Seas, the difference in Ekman transport is directed toward Fram Strait and the Barents Sea Opening; in the northern Barents Sea, the difference in transport is directed toward the central Arctic (Figures 7d and 7f). In the albedo experiment, the differences in Ekman transport are relatively small and are directed from the Eurasian Basin toward the central Arctic. North of Fram Strait, there is a small area with Ekman convergence (Figure 7e).

In the Arctic Ocean, the differences in Ekman transports lead to a redistribution of low salinity ocean surface water. Halosteric height differences, i.e., the component of change in sea-surface height induced by differences in freshwater content in the water column, are shown in Figures 8a–8c. Regions of Ekman-transport-driven freshwater convergence (or divergence) show an increase (or decrease) in halosteric height. In both the wind replacement and the albedo reduction experiments, two regions of increased halosteric height emerge: the Canadian Basin, where freshwater is shifted from the boundaries toward the center; and the Eurasian Basin, where increases in halosteric height are visible north of Fram Strait. Decreases in

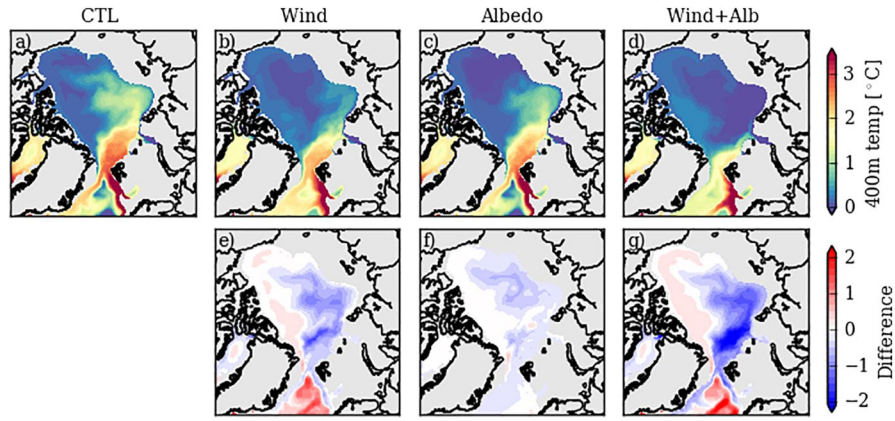

Figure 9. Mean temperature [ºC] for the control simulation (a) and the sensitivity experiments (b–d) at 400 m depth and the respective temperature differences between the sensitivity experiments and the control simulation [°C] (e–g). The results are averaged over the last 10 years of the simulations (1980–1989).

halosteric height are visible north of the Barents and Kara seas and in the Nordic Seas. Overall, the halosteric height differences are smaller in the albedo scenario. But the sea-ice reduction amplifies the effect of wind perturbation in the third sensitivity experiment, in which both perturbations were applied.

The differences in total sea surface height between the sensitivity runs and the control run are shown in Figures 8d–8f. The comparison of halosteric height differences (Figures 7a–7c) to sea surface height differences (Figures 8d–8f) shows similar patterns for the central Arctic Ocean, in Baffin Bay and in the Barents and Kara seas. The resulting indication is that sea surface height changes are driven by freshwater distribution changes in those regions. For the experiments WIND and WIND + ALB, however, the halosteric height in the Nordic Seas has decreased while sea surface height has increased (compare Figures 8a–8c and Figures 8c–8f). The increase in sea surface height, then, is not due to salinity changes but rather due to warmer temperatures (Figures 9e and 9g, Nordic Sea region), that is, to thermosteric height changes.

These differences in sea surface height lead to differences in surface geostrophic velocity. In the WIND experiment, the velocity anomaly is anticyclonic over the Arctic basin and south of Fram Strait; in the Nordic Seas, the velocity anomaly is anticyclonic too (Figure 8g). Just north of Fram Strait, the difference in geostrophic surface current points westward. In the ALBEDO experiment, there is also an anticyclonic surface geostrophic current anomaly, this one mostly confined to the Canadian Basin (Figure 8h). In the Eurasian Basin, there is a weak cyclonic anomaly in surface geostrophic velocity. The effect of the wind replacement is amplified again by sea-ice decline in the experiment in which wind and albedo are considered together (Figure 8i).

Finally, the effect of applying the wind from the coupled model and reducing sea ice cover on the horizontal temperature distribution at 400 m depth is evaluated (Figure 9). Compared to the control run, applying the wind from the coupled model leads to colder temperatures both north of Fram Strait and along the cyclonic boundary current pathway. Warmer temperatures can be seen along the Greenland and Canadian slope and in the Greenland Sea (Figure 9e).

In the ALBEDO experiment, a slight cold bias has developed along the deep boundary current pathway; it is most pronounced at the intersection of the Eurasian Basin, the Lomonosov Ridge and the Canadian Basin, and also in the Greenland Sea (Figure 9f). When wind replacement and albedo reduction are combined, the cold biases grow more pronounced (Figure 9g); in fact, here the warm AW is no longer visible in the boundary current beyond the Barents Sea (Figure 9d). Instead, there is a cold pool in the Eurasian Basin and warmer temperatures north of Greenland and the Canadian Arctic Archipelago as well as along the southern boundary of the Canadian Basin; together, these imply an anticyclonic reversal of the AW flow (Figure 9d). The biased temperature distribution shown in Figure 9d is remarkably similar to the one in the coupled set-up (Figure 2b), and it is thereby with greater confidence that biases in the coupled system can be explained by analyzing the sensitivity experiments in an ocean-only configuration.

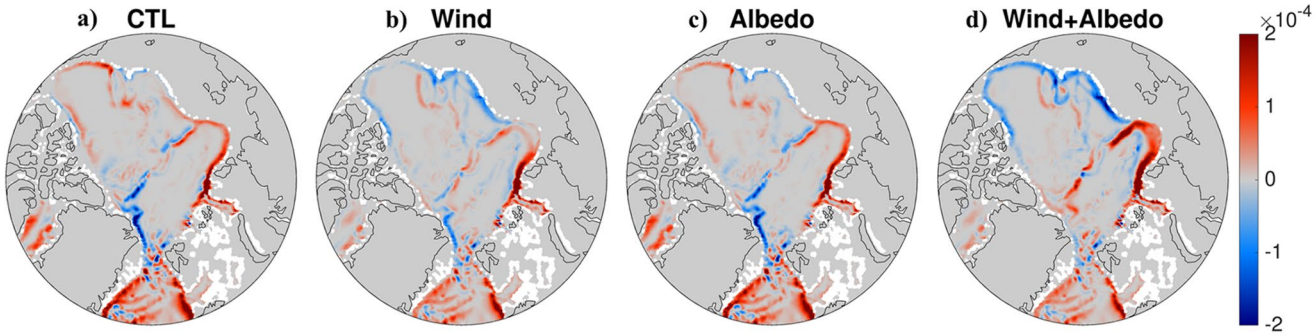

Figure 10. Mean topostrophy below 280 m depth [m²/s] for the control simulation and the three sensitivity experiments averaged over the last 10 years of simulation (1980–1989). Red indicates cyclonic circulation, and blue indicates anticyclonic circulation.

4. Discussion

The sensitivity experiments performed with the forced ocean–sea-ice model show that biases like the ones in AWI-CM1, which affect surface pressure and wind field over the Arctic, paired with underestimation of the sea-ice cover, together can result in an unrealistic temperature distribution at 400 m depth. In such a case, the warm AW is no longer visible in the boundary current beyond the Barents Sea; instead, a cold pool emerges in the eastern Eurasian Basin. And at the same time, warmer temperatures appear both along the western boundary of the Arctic Ocean and in the Greenland Sea south of Fram Strait. These changes imply that some of the AW that does enter the Arctic Ocean is directed westwards and circulates anticyclonically around the Canadian Basin; the same changes also imply that less of the warm AW propagates from the Nordic Seas into the Arctic Ocean.

To investigate the westward direction and anticyclonic circulation of a portion of the AW around the Canadian Basin, we computed the depth-average topostrophy between 300 m and 3,000 m. The concept of topostrophy was introduced as part of the Arctic Ocean Model Intercomparison Project (AOMIP, Proshutinsky et al., 2001) by Holloway et al. (2007) in order to compare the simulated circulation between models. The velocity vector field is reduced to a scalar quantity τ that characterizes the tendency of a current to follow topographic slopes:

$$\tau = \left(V \times \nabla D\right)z, \tag{1}$$

where **V** is velocity, D is the depth gradient, and **z** is the unit vertical vector. A positive value indicates a current with shallower water to the right (northern hemisphere). In the case of the Arctic Circumpolar Boundary Current, positive topostrophy indicates a cyclonic flow direction. The control simulation shows a mostly cyclonic flow all around the Arctic Ocean Basin except for in a small area north of Greenland (Figure 10a). With wind forcing from the coupled model, the circulation in the Canadian Basin turns anticyclonic (Figure 10b), a shift that is most prominent on the East Siberian side. In the ALBEDO experiment, the direction of the circulation over continental slopes is barely affected; only north of the East Siberian Sea does the current have a slightly higher anticyclonic tendency (Figure 10c). In the experiment WIND + ALB, the circulation in most of the Canadian Basin is clearly anticyclonic whereas the cyclonic circulation in the Eurasian Basin seems strengthened (Figure 10d).

The mean net volume transport through the Barents Sea Opening is higher in the WIND (2.4 Sv) and WIND + ALB (2.7 SV) experiments than in the CTL (2.1 Sv) and ALB (2.3 Sv) experiments. These changes are associated with a reduced SSH in the northern Barents Sea (Figure 8). The AW loses most of its heat in the Barents Sea region before entering the Arctic deep basin (Smedsrud et al., 2013), so the increased AW transport through the BSO strengthens the cyclonic boundary circulation in the eastern Eurasian Basin (Figure 10), but it rather feeds more cold water to the ACBC (Figure 9d). This effect is most prominent in the WIND + ALB experiment, which has the strongest increase in BSO inflow.

Looking at the topostrophy in the Nordic Seas (Figure 10), we see that both of the simulations that feature replaced wind forcing show the West Spitsbergen Current (WSC) and the East Greenland Current (EGC) as weaker than they are in the control simulation.

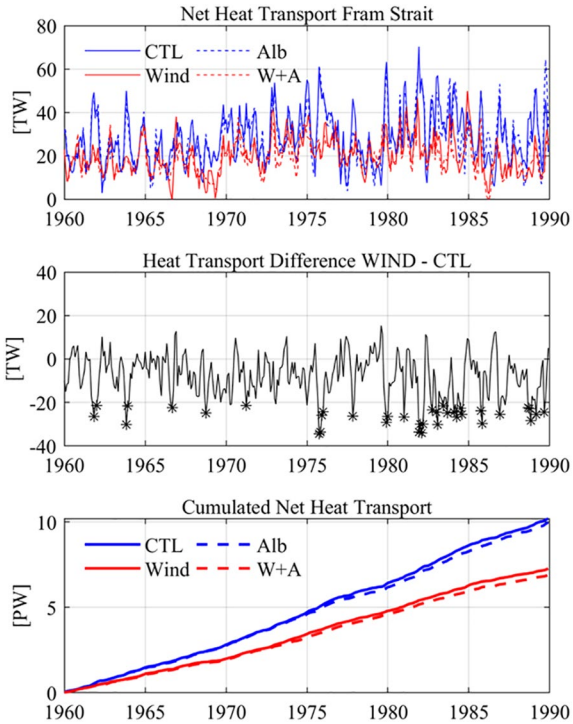

Figure 11. Time series of monthly net heat transport [TW] through Fram Strait for all experiments (a), difference in heat transport [TW] between experiment "Wind" and "CTL," with months below the 10th percentile marked with stars (b), cumulated net Fram Strait heat transport [TW] for all experiments (c).

Next, we looked at volume (not shown) and heat transport through Fram Strait across a section at 79°N. The mean monthly net flow of heat through Fram Strait into the Arctic is higher for both the control simulation (28.3 TW) and the ALBEDO experiment (27.7 TW) than it is for the WIND (20.2 TW) and WIND + ALB (19.1 TW) experiments (Figures 11a). Accumulated over 32 years of simulation, the net heat transport into the Arctic is 29% less in the WIND experiment and 32% less in the WIND + ALB experiment (Figures 11c).

The monthly difference in net heat transport into the Arctic between the WIND experiment and CTL is shown in Figures 11b. Most of the time, monthly net heat transport through Fram Strait in the control simulation is larger; this can be explained by the wind bias over the Nordic Seas (Figure 12). Chatterjee et al. (2018) investigated the impact of the Greenland Sea Gyre (GSG) circulation on AW temperature variability at Fram Strait based on ocean reanalysis data and found that cold anomalies at Fram Strait are related to an atmospheric pattern that shows a high-pressure anomaly centered over Svalbard, northerly winds over the western Greenland Sea, and southerly wind along the Norwegian coast (Chatterjee et al., 2018, see their Figure 3c). Such a wind pattern, which resembles the model bias in AWI-CM1, leads to Ekman convergence in the GSG and positive sea surface height anomalies which weaken the cyclonic GSG circulation. Figure 8d shows the difference in SSH between the WIND experiment and the control run as a positive height difference in the Nordic Seas. A composite (not shown) of SSH differences for the months with the largest negative net heat transport differences (Figure 10b, starred months show the 10th percentile) exhibits even higher SSH differences. The increased SSH in the Nordic Seas reduces AW transport to the Nordic Seas across the Iceland-Scotland Ridge. Therefore, the wind anomaly both reduces AW transport toward the Arctic Ocean and increases the amount of AW entering the Arctic through the BSO. As a consequence, there is both a reduction in AW transport in the West Spitsbergen Current at Fram Strait as well as a reduction in AW recirculation in the EGC.

Because we set out to understand the influence of large-scale wind biases in a coupled model, we did not, for the sensitivity experiments, separate the wind bias into local (over the central Arctic) and remote (over the Nordic Seas) components. Nonetheless, the results discussed above are consistent with previous model studies on the role of local and remote wind forcing for the ACBC. Lique et al. (2015) and Lique and Johnson (2015) studied the effects of local and remote wind forcing on AW circulation at depth; they found that remote wind forcing over the Nordic Seas and the Barents Sea can cause a rapid, direct response in the AW circulation in the Arctic Ocean through a change in AW inflow. At the same time, they found that local wind forcing over the Canadian Basin results in slower changes that are "filtered" through surface circulation, which in turn modulates the deeper AW circulation. Here, a stronger anticyclonic wind forces a strong, deep Beaufort Gyre in the same direction such that no deep counterflow can develop.

Although the bias in sea-ice cover does not affect net heat transport through Fram Strait (Figures 11c), the sensitivity experiment with reduced albedo shows that reduced sea-ice cover does influence the surface distribution of freshwater (Figure 8b). Though reduced sea-ice cover has less of an effect than the wind bias has, it too contributes to a strengthening of the anticyclonic surface current in the western Arctic (Figure 8h). This effect of sea-ice decline on surface dynamics in the Arctic Ocean was also apparent in Wang et al. (2019). Spall (2013), based on idealized model simulations, had already shown that when the ice–ocean stress was removed completely, anticyclonic circulation in the Canadian Basin is lost and eddy fluxes from the boundary are enhanced, which indicates that the instability of the boundary current is suppressed by ice cover. Ideally, this potential consequence of sea-ice decline, and any related feedback should be investigated further using skillful coupled models to project future Arctic conditions.

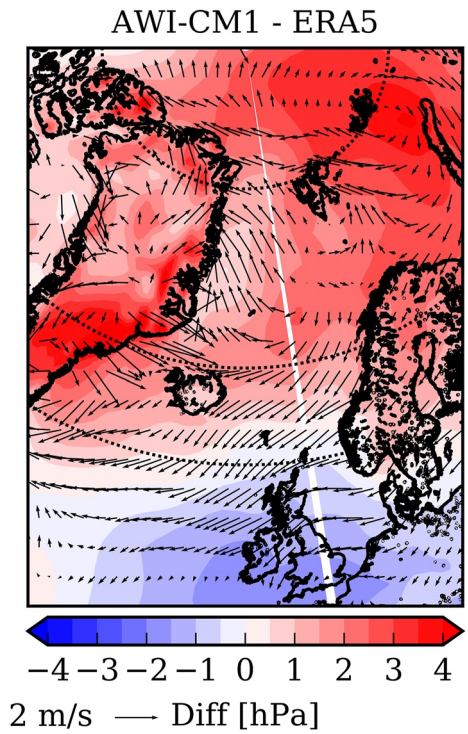

Figure 12. Bias in MSLP [hPa] and wind in AWI-CM1 compared to ERA5 with focus on the Nordic Seas.

This study has investigated effects of a SLP and wind bias that are specific to the coupled climate model AWI-CM1. It is worth stressing that this particular bias is not unique to AWI-CM1: Another CMIP6 model, MPI-ESM, which also employs ECHAM6.3 as its atmospheric component but which has a different ocean–sea-ice component, shows a SLP bias nearly identical both in shape and magnitude. Furthermore, such a SLP bias has been found in other atmospheric models (Koenigk et al., 2013). Indeed, it is the dominant feature in multi-model means of SLP bias in model intercomparison studies of coupled and uncoupled models (Walsh et al., 2002). It has been suggested that the truncation of the North Atlantic storm track in the models, which prevents Atlantic cyclones from moving further north and into the region of the Norwegian Sea, Barents Sea, and Kara Sea, is what causes this bias. It has also been suggested that biased surface winds in the Arctic can adversely affect sea-ice transport, the resulting distribution of sea-ice concentration and thickness, and the export of ice and freshwater into the North Atlantic (Chapman & Walsh, 2007; Walsh et al., 2002). Our study shows that this wind bias pattern can additionally affect simulated circulation in the deep Arctic Ocean by imposing an anticyclonic surface circulation anomaly that then imprints on the deeper ocean circulation. Our results also reveal that a negative sea-ice bias could amplify this issue.

Walsh et al. (2002) recommended that efforts to ameliorate the SLP bias in atmospheric models should focus on representing the topography across northern Asia and Greenland, or, more specifically, on topographic parameterizations which could affect the exchange of mass between Asia and the Arctic. They noted that the resolution of the atmospheric model may in part determine the magnitude of the bias. For AWI-CM1, we tried tuning some parameters related to model topography (gk_wake, gk_drag, and gk_lift) but without obtaining a significant reduction in the SLP or AW circulation bias.

Mu et al. (2020) showed that the assimilation of sea surface temperature (SST) into AWI-CM1 led to a more realistic atmospheric circulation and also reversed the erroneous direction of the deep boundary current carrying AW after 8 simulation years with data assimilation. This reversal of the current into a cyclonic flow was attributed to the improvement of atmospheric states over the ice-free area that can further propagate to the whole Arctic dynamically.

5. Conclusions

Atlantification might be an important driver in amplified Arctic sea-ice melting and Arctic Ocean warming (Årthun et al., 2019) as well as in regional differences in sea-ice loss (Årthun et al., 2021). Using global coupled climate models to study the evolution of Atlantification and any associated feedback in the Arctic climate system requires realistic simulations of AW inflow and circulation through the Arctic Ocean. A skill assessment of the AW layer representations in the CMIP5 (Shu et al., 2019) and CMIP6 (Khosravi et al., 2021) models shows that, in many of the models that do simulate a distinct Arctic AW layer, this layer is too thick, too deep, or does not show the observed warming trend. Biases like this are commonly related to insufficient resolution, too much mixing in the ocean component, and unrealistic Atlantic-Arctic Ocean exchanges.

Our study shows that even if all impediments to realistically simulating AW are addressed in the ocean model (e.g., by implementing sufficient resolution in the horizontal and vertical, Arctic gateways-resolving grid resolution, faithful bathymetry representation, the right amount of mixing), new obstacles may arise when the ocean model is coupled to an atmosphere model with its own shortcomings in the Arctic. AWI-CM1, like many other coupled climate models, exhibits a bias in SLP over the Arctic Ocean, with higher pressures over the Eurasian Basin and the Barents and Kara Seas and lower SLP over the Canadian

Basin. In the Arctic Ocean, the bias in wind stress (which is related to the biased surface pressure gradient) leads to differences in Ekman transport, freshwater distribution, and halosteric height that strengthen the anticyclonic surface circulation in the Canadian Basin to the point of reversing the deep counterflow. This effect is visualized by the negative topostrophy (Figures 10b and 10d) and warm bias (Figures 9e and 9g) in the Canadian Basin. An underestimation of sea-ice concentration such as is seen in AWI-CM1 can amplify the described processes locally. In the Nordic Seas, an anticyclonic wind bias increases the SSH and weakens the cyclonic gyre circulation, which leads to reduced volume and heat (a proxy for AW) transport into the Arctic Ocean through Fram Strait. At the same time, the wind bias increases AW transport through the BSO. And since the BSO feeds cold water to the deep basin, the overall effect is a cold bias in the Eurasian Basin (Figures 9e and 9g).

The problem of biased SLP over the Arctic cannot be overcome easily. Efforts as suggested by Walsh et al. (2002) to tune parameters related to model topography did not lead to a significant reduction of the SLP bias or the circulation bias in our practice. SST assimilation seems to rectify the circulation in AWI-CM1, but this constraint cannot of course be applied to the future scenario simulations.

Currently, a new version (version 3) of AWI-CM is in development. For its atmospheric component, ECHAM is replaced with OpenIFS (OIFS, Roberts et al., 2018). Preliminary results show that the SLP bias pattern over the Arctic is present in OIFS, too, but it is of smaller magnitude than in ECHAM. The temperature distribution at 400 m implies a cyclonic circumpolar circulation in simulations with AWI-CM3. This new model version has yet to be released and will be described later, and separately, after the initial model tuning process.

The Arctic is a hotspot in global warming, but there is still a large inter-model spread as well as model uncertainty in CMIP6 projections of the surface warming–especially in the Arctic (Cai et al., 2021). Detailed investigations of model biases are needed to improve the simulations and reduce sources of model uncertainty. Simulating ocean heat transport into and within the Arctic more faithfully will help to understand and better predict the course of change in the Arctic.

Data Availability Statement

The model data used to produce the figures are available at https://doi.org/10.5281/zenodo.5139756. Our model simulations were compared to the Polar science center Hydrographic Climatology (PHC) version 3.0 (available at http://psc.apl.washington.edu/nonwp_projects/PHC/Climatology.html), to ERA5 reanalysis data (downloaded from the Copernicus data store at https://cds.climate.copernicus.eu/cdsapp#!/home), and sea-ice concentration data from the National Snow & Ice Data Center (https://nsidc.org/). The simulations were performed at the German Climate Computing Center (DKRZ) using ESM-Tools (https://www.esm-tools.net/).

Acknowledgments
C. Hinrichs, T. Semmler, and T. Jung received funding from the European Union's Horizon 2020 Research and Innovation program, through grant agreement No. 727862 APPLICATE. This is a contribution to the Year of Polar Prediction (YOPP), a flagship activity of the Polar Prediction Project (PPP) initiated by the World Weather Research Programme (WWRP) of the World Meteorological Organization (WMO). We acknowledge the WMO WWRP for its role in coordinating this international research activity. The work described in this paper has also received funding from the Helmholtz Association through the project "Regional Climate Change (REKLIM)" and "Advanced Earth System Model Capacity." Open access funding enabled and organized by Projekt DEAL.

References

Aagaard, K. (1989). *A synthesis of the Arctic Ocean circulation*. Le Conseil.
Årthun, M., & Eldevik, T. (2016). On anomalous ocean heat transport toward the Arctic and associated climate predictability. *Journal of Climate*, *29*(2), 689–704. https://doi.org/10.1175/jcli-d-15-0448.1
Årthun, M., Eldevik, T., & Smedsrud, L. H. (2019). The role of Atlantic heat transport in future Arctic winter sea ice loss. *Journal of Climate*, *32*(11), 3327–3341. https://doi.org/10.1175/jcli-d-18-0750.1
Årthun, M., Onarheim, I. H., Dörr, J., & Eldevik, T. (2021). The Seasonal and Regional Transition to an Ice-Free Arctic. *Geophysical Research Letters*, *48*(1), e2020GL090825. https://doi.org/10.1029/2020GL090825
Asbjørnsen, H., Årthun, M., Skagseth, Ø., & Eldevik, T. (2020). Mechanisms Underlying Recent Arctic Atlantification. *Geophysical Research Letters*, *47*(15), e2020GL088036. https://doi.org/10.1029/2020GL088036
Barton, B. I., Lenn, Y.-D., & Lique, C. (2018). Observed Atlantification of the Barents Sea causes the polar front to limit the expansion of winter sea ice. *Journal of Physical Oceanography*, *48*(8), 1849–1866. https://doi.org/10.1175/jpo-d-18-0003.1
Beszczynska-Möller, A., Fahrbach, E., Schauer, U., & Hansen, E. (2012). Variability in Atlantic water temperature and transport at the entrance to the Arctic Ocean, 1997–2010. *ICES Journal of Marine Science*, *69*(5), 852–863. https://doi.org/10.1093/icesjms/fss056
Boitsov, V. D., Karsakov, A. L., & Trofimov, A. G. (2012). Atlantic water temperature and climate in the Barents Sea, 2000–2009. *ICES Journal of Marine Science*, *69*(5), 833–840. https://doi.org/10.1093/icesjms/fss075
Cai, Z., You, Q., Wu, F., Chen, H. W., Chen, D., & Cohen, J. (2021). Arctic warming revealed by multiple CMIP6 models: Evaluation of historical simulations and quantification of future projection uncertainties. *Journal of Climate*, *34*, 1–52. https://doi.org/10.1175/jcli-d-20-0791.1

Cavalieri, D. J., Parkinson, C. L., Gloersen, P., & Zwally, H. J. (1996). *Sea Ice concentrations from nimbus-7 SMMR and DMSP SSM/I-SSMIS passive microwave data*. Version 1.
Chapman, W. L., & Walsh, J. E. (2007). Simulations of Arctic temperature and pressure by global coupled models. *Journal of Climate*, *20*(4), 609–632. https://doi.org/10.1175/jcli4026.1
Charnock, H. (1955). Wind stress on a water surface. *Quarterly Journal of the Royal Meteorological Society*, *81*(350), 639–640. https://doi.org/10.1002/qj.49708135027
Chatterjee, S., Raj, R. P., Bertino, L., Skagseth, Ø., Ravichandran, M., & Johannessen, O. M. (2018). Role of Greenland sea gyre circulation on Atlantic water temperature variability in the Fram Strait. *Geophysical Research Letters*, *0*(0), 8399, 8406. https://doi.org/10.1029/2018GL079174
Cohen, J., Zhang, X., Francis, J., Jung, T., Kwok, R., Overland, J., et al. (2020). Divergent consensuses on Arctic amplification influence on midlatitude severe winter weather. *Nature Climate Change*, *10*(1), 20–29. https://doi.org/10.1038/s41558-019-0662-y
Danilov, S., Wang, Q., Timmermann, R., Iakovlev, N., Sidorenko, D., Kimmritz, M., et al. (2015). Finite-Element Sea Ice Model (FESIM), version 2. *Geoscientific Model Development*, *8*(6), 1747–1761. https://doi.org/10.5194/gmd-8-1747-2015
Dmitrenko, I. A., Polyakov, I. V., Kirillov, S. A., Timokhov, L. A., Frolov, I. E., Sokolov, V. T., et al. (2008). Toward a warmer Arctic Ocean: Spreading of the early 21st century Atlantic Water warm anomaly along the Eurasian Basin margins. *Journal of Geophysical Research*, *113*(C5). https://doi.org/10.1029/2007jc004158
Furevik, T. (2001). Annual and interannual variability of Atlantic Water temperatures in the Norwegian and Barents Seas: 1980–1996. *Deep Sea Research Part I: Oceanographic Research Papers*, *48*(2), 383–404. https://doi.org/10.1016/S0967-0637(00)00050-9
Golubeva, E., & Platov, G. (2007). On improving the simulation of Atlantic Water circulation in the Arctic Ocean. *Journal of Geophysical Research*, *112*(C4). https://doi.org/10.1029/2006jc003734
Good, S. A., Martin, M. J., & Rayner, N. A. (2013). EN4: Quality controlled ocean temperature and salinity profiles and monthly objective analyses with uncertainty estimates. *Journal of Geophysical Research: Oceans*, *118*(12), 6704–6716. https://doi.org/10.1002/2013jc009067
Griffies, S. M., Biastoch, A., Böning, C., Bryan, F., Danabasoglu, G., Chassignet, E. P., et al. (2009). Coordinated Ocean-ice Reference Experiments (COREs). *Ocean Modelling*, *26*(1), 1–46. https://doi.org/10.1016/j.ocemod.2008.08.007
Hátún, H., Sandø, A. B., Drange, H., Hansen, B., & Valdimarsson, H. (2005). Influence of the Atlantic Subpolar Gyre on the Thermohaline Circulation. *Science*, *309*(5742), 1841–1844. https://doi.org/10.1126/science.1114777
Hersbach, H., Bell, B., Berrisford, P., Hirahara, S., Horányi, A., Muñoz-Sabater, J., et al. (2020). The ERA5 global reanalysis. *Quarterly Journal of the Royal Meteorological Society*, *146*(730), 1999–2049. https://doi.org/10.1002/qj.3803
Holliday, N. P., Hughes, S. L., Bacon, S., Beszczynska-Möller, A., Hansen, B., Lavín, A., et al. (2008). Reversal of the 1960s to 1990s freshening trend in the northeast North Atlantic and Nordic Seas. *Geophysical Research Letters*, *35*(3). https://doi.org/10.1029/2007GL032675
Holloway, G., Dupont, F., Golubeva, E., Häkkinen, S., Hunke, E., Jin, M., et al. (2007). Water properties and circulation in Arctic Ocean models. *Journal of Geophysical Research: Oceans*, *112*(C4). https://doi.org/10.1029/2006jc003642
Holloway, G., & Wang, Z. (2009). Representing eddy stress in an Arctic Ocean model. *Journal of Geophysical Research*, *114*(C6). https://doi.org/10.1029/2008jc005169
Ilıcak, M., Drange, H., Wang, Q., Gerdes, R., Aksenov, Y., Bailey, D., et al. (2016). An assessment of the Arctic Ocean in a suite of interannual CORE-II simulations. Part III: Hydrography and fluxes. *Ocean Modelling*, *100*, 141–161. https://doi.org/10.1016/j.ocemod.2016.02.004
Itkin, P., Karcher, M., & Gerdes, R. (2014). Is weaker Arctic sea ice changing the Atlantic water circulation? *Journal of Geophysical Research: Oceans*, *119*(9), 5992–6009. https://doi.org/10.1002/2013jc009633
Ivanov, V., Smirnov, A., Alexeev, V., Koldunov, N. V., Repina, I., & Semenov, V. (2018). Contribution of convection-induced heat flux to winter ice decay in the Western Nansen Basin. *Journal of Geophysical Research: Oceans*, *123*(9), 6581–6597. https://doi.org/10.1029/2018jc013995
Jung, T., Gordon, N. D., Bauer, P., Bromwich, D. H., Chevallier, M., Day, J. J., et al. (2016). Advancing polar prediction capabilities on daily to seasonal time scales. *Bulletin of the American Meteorological Society*, *97*(9), 1631–1647. https://doi.org/10.1175/bams-d-14-00246.1
Karcher, M., Kauker, F., Gerdes, R., Hunke, E., & Zhang, J. (2007). On the dynamics of Atlantic Water circulation in the Arctic Ocean. *Journal of Geophysical Research*, *112*(C4). https://doi.org/10.1029/2006jc003630
Khosravi, N., Wang, Q., Koldunov, N., Hinrichs, C., Semmler, T., Danilov, S., & Jung, T. (2021). Arctic Ocean in CMIP6 Models: Historical and projected temperature and salinity in the deep basins. *Earth's Future*, [preprint]. https://doi.org/10.1002/essoar.10507417.1
Koenigk, T., & Brodeau, L. (2014). Ocean heat transport into the Arctic in the twentieth and twenty-first century in EC-Earth. *Climate Dynamics*, *42*(11), 3101–3120. https://doi.org/10.1007/s00382-013-1821-x
Koenigk, T., Brodeau, L., Graversen, R. G., Karlsson, J., Svensson, G., Tjernström, M., et al. (2013). Arctic climate change in 21st century CMIP5 simulations with EC-Earth. *Climate Dynamics*, *40*(11), 2719–2743. https://doi.org/10.1007/s00382-012-1505-y
Koldunov, N. V., Aizinger, V., Rakowsky, N., Scholz, P., Sidorenko, D., Danilov, S., & Jung, T. (2019). Scalability and some optimization of the Finite-volumE Sea ice–Ocean Model, Version 2.0 (FESOM2). *Geoscientific Model Development*, *12*(9), 3991–4012. https://doi.org/10.5194/gmd-12-3991-2019
Large, W. G., & Yeager, S. (2009). The global climatology of an interannually varying air–sea flux data set. *Climate Dynamics*, *33*(2–3), 341–364. https://doi.org/10.1007/s00382-008-0441-3
Lique, C., & Johnson, H. L. (2015). Is there any imprint of the wind variability on the Atlantic Water circulation within the Arctic Basin? *Geophysical Research Letters*, *42*(22), 9880–9888. https://doi.org/10.1002/2015gl066141
Lique, C., Johnson, H. L., & Davis, P. E. D. (2015). On the interplay between the circulation in the surface and the intermediate layers of the Arctic Ocean. *Journal of Physical Oceanography*, *45*(5), 1393–1409. https://doi.org/10.1175/jpo-d-14-0183.1
Maqueda, M. M., & Holloway, G. (2006). Second-order moment advection scheme applied to Arctic Ocean simulation. *Ocean Modelling*, *14*(3–4), 197–221. https://doi.org/10.1016/j.ocemod.2006.05.003
Mu, L., Nerger, L., Tang, Q., Loza, S. N., Sidorenko, D., Wang, Q., et al. (2020). Toward a data assimilation system for seamless sea ice prediction based on the AWI climate model. *Journal of Advances in Modeling Earth Systems*, *12*(4), e2019MS001937. https://doi.org/10.1029/2019ms001937
Müller, W. A., Jungclaus, J. H., Mauritsen, T., Baehr, J., Bittner, M., Budich, R., et al. (2018). A Higher-resolution Version of the Max Planck Institute Earth System Model (MPI-ESM1. 2-HR). *Journal of Advances in Modeling Earth Systems*, *10*(7), 1383–1413. https://doi.org/10.1029/2017ms001217
Nazarenko, L., Holloway, G., & Tausnev, N. (1998). Dynamics of transport of "Atlantic signature" in the Arctic Ocean. *Journal of Geophysical Research*, *103*(C13), 31003–31015. https://doi.org/10.1029/1998jc900017
Olonscheck, D., Mauritsen, T., & Notz, D. (2019). Arctic sea-ice variability is primarily driven by atmospheric temperature fluctuations. *Nature Geoscience*, *12*(6), 430–434. https://doi.org/10.1038/s41561-019-0363-1

Onarheim, I. H., Smedsrud, L. H., Ingvaldsen, R. B., & Nilsen, F. (2014). Loss of sea ice during winter north of Svalbard. *Tellus A: Dynamic Meteorology and Oceanography*, *66*(1), 23933. https://doi.org/10.3402/tellusa.v66.23933

Polyakov, I. V., Beszczynska, A., Carmack, E. C., Dmitrenko, I. A., Fahrbach, E., Frolov, I. E., et al. (2005). One more step toward a warmer Arctic. *Geophysical Research Letters*, *32*(17). https://doi.org/10.1029/2005gl023740

Polyakov, I. V., Bhatt, U. S., Walsh, J. E., Abrahamsen, E. P., Pnyushkov, A. V., & Wassmann, P. F. (2013). Recent oceanic changes in the Arctic in the context of long-term observations. *Ecological Applications*, *23*(8), 1745–1764. https://doi.org/10.1890/11-0902.1

Polyakov, I. V., Pnyushkov, A. V., Alkire, M. B., Ashik, I. M., Baumann, T. M., Carmack, E. C., et al. (2017). Greater role for Atlantic inflows on sea-ice loss in the Eurasian Basin of the Arctic Ocean. *Science*, *356*(6335), 285–291. https://doi.org/10.1126/science.aai8204

Polyakov, I. V., Rippeth, T. P., Fer, I., Alkire, M. B., Baumann, T. M., Carmack, E. C., et al. (2020). Weakening of Cold halocline layer exposes sea ice to oceanic heat in the eastern Arctic Ocean. *Journal of Climate*, *33*(18), 8107–8123. https://doi.org/10.1175/jcli-d-19-0976.1

Proshutinsky, A., Steele, M., Zhang, J., Holloway, G., Steiner, N., Häkkinen, S., et al. (2001). The Arctic Ocean Model Intercomparison Project (AOMIP). *Eos Transactions American Geophysical Union*, *82*(51), 637–637. https://doi.org/10.1029/01eo00365

Rackow, T., Goessling, H. F., Jung, T., Sidorenko, D., Semmler, T., Barbi, D., & Handorf, D. (2016). Towards multi-resolution global climate modeling with ECHAM6-FESOM. Part II: Climate variability. *Climate Dynamics*, *50*, 1–26. https://doi.org/10.1007/s00382-016-3192-6

Roberts, C. D., Senan, R., Molteni, F., Boussetta, S., Mayer, M., & Keeley, S. P. (2018). Climate model configurations of the ECMWF Integrated Forecasting System (ECMWF-IFS cycle 43r1) for HighResMIP. *Geoscientific Model Development*, *11*(9), 3681–3712. https://doi.org/10.5194/gmd-11-3681-2018

Rudels, B., Friedrich, H. J., & Quadfasel, D. (1999). The Arctic circumpolar boundary current. *Deep Sea Research Part II: Topical Studies in Oceanography*, *46*(6–7), 1023–1062. https://doi.org/10.1016/s0967-0645(99)00015-6

Semmler, T., Danilov, S., Gierz, P., Goessling, H. F., Hegewald, J., Hinrichs, C., et al. (2020). Simulations for CMIP6 With the AWI Climate Model AWI-CM-1-1. *Journal of Advances in Modeling Earth Systems*, *12*(9), e2019MS002009. https://doi.org/10.1029/2019MS002009

Serreze, M., Barrett, A., Stroeve, J., Kindig, D., & Holland, M. (2009). The emergence of surface-based Arctic amplification. *The Cryosphere*, *3*(1), 11–19. https://doi.org/10.5194/tc-3-11-2009

Serreze, M. C., & Barry, R. G. (2011). Processes and impacts of Arctic amplification: A research synthesis. *Global and Planetary Change*, *77*(1–2), 85–96. https://doi.org/10.1016/j.gloplacha.2011.03.004

Shu, Q., Wang, Q., Song, Z., & Qiao, F. (2021). The poleward enhanced Arctic Ocean cooling machine in a warming climate. *Nature Communications*, *12*(1), 2966. https://doi.org/10.1038/s41467-021-23321-7

Shu, Q., Wang, Q., Su, J., Li, X., & Qiao, F. (2019). Assessment of the Atlantic water layer in the Arctic Ocean in CMIP5 climate models. *Climate Dynamics*, *53*(9), 5279–5291. https://doi.org/10.1007/s00382-019-04870-6

Sidorenko, D., Rackow, T., Jung, T., Semmler, T., Barbi, D., Danilov, S., et al. (2015). Towards multi-resolution global climate modeling with ECHAM6–FESOM. Part I: Model formulation and mean climate. *Climate Dynamics*, *44*(3–4), 757–780. https://doi.org/10.1007/s00382-014-2290-6

Smedsrud, L. H., Esau, I., Ingvaldsen, R. B., Eldevik, T., Haugan, P. M., Li, C., et al. (2013). The role of the Barents Sea in the Arctic climate system. *Reviews of Geophysics*, *51*(3), 415–449. https://doi.org/10.1002/rog.20017

Spall, M. A. (2013). On the Circulation of Atlantic Water in the Arctic Ocean. *Journal of Physical Oceanography*, *43*(11), 2352–2371. https://doi.org/10.1175/jpo-d-13-079.1

Steele, M., Morley, R., & Ermold, W. (2001). PHC: A global ocean hydrography with a high-quality Arctic Ocean. *Journal of Climate*, *14*(9), 2079–2087. https://doi.org/10.1175/1520-0442(2001)014<2079:pagohw>2.0.co;2

Stevens, B., Giorgetta, M., Esch, M., Mauritsen, T., Crueger, T., Rast, S., et al. (2013). Atmospheric component of the MPI-M Earth System Model: ECHAM6. *Journal of Advances in Modeling Earth Systems*, *5*(2), 146–172. https://doi.org/10.1002/jame.20015

Timmermans, M.-L., & Marshall, J. (2020). Understanding Arctic Ocean circulation: A review of ocean dynamics in a changing climate. *Journal of Geophysical Research: Oceans*, *125*(4), e2018JC014378. https://doi.org/10.1029/2018jc014378

Vihma, T. (2014). Effects of Arctic sea ice decline on weather and climate: A review. *Surveys in Geophysics*, *35*(5), 1175–1214. https://doi.org/10.1007/s10712-014-9284-0

Wallace, J. M., Held, I. M., Thompson, D. W., Trenberth, K. E., & Walsh, J. E. (2014). Global warming and winter weather. *Science*, *343*(6172), 729–730. https://doi.org/10.1126/science.343.6172.729

Walsh, J. E., Kattsov, V. M., Chapman, W. L., Govorkova, V., & Pavlova, T. (2002). Comparison of Arctic climate simulations by uncoupled and coupled global models. *Journal of Climate*, *15*(12), 1429–1446. https://doi.org/10.1175/1520-0442(2002)015<1429:coacsb>2.0.co;2

Wang, Q., Danilov, S., Sidorenko, D., Timmermann, R., Wekerle, C., Wang, X., et al. (2014). The Finite Element Sea Ice-Ocean Model (FESOM) v. 1.4: Formulation of an ocean general circulation model. *Geoscientific Model Development*, *7*(2), 663–693. https://doi.org/10.5194/gmd-7-663-2014

Wang, Q., Ilicak, M., Gerdes, R., Drange, H., Aksenov, Y., Bailey, D. A., et al. (2016a). An assessment of the Arctic Ocean in a suite of interannual CORE-II simulations. Part I: Sea ice and solid freshwater. *Ocean Modelling*, *99*, 110–132. https://doi.org/10.1016/j.ocemod.2015.12.008

Wang, Q., Ilicak, M., Gerdes, R., Drange, H., Aksenov, Y., Bailey, D. A., et al. (2016b). An assessment of the Arctic Ocean in a suite of interannual CORE-II simulations. Part II: Liquid freshwater. *Ocean Modelling*, *99*, 86–109. https://doi.org/10.1016/j.ocemod.2015.12.009

Wang, Q., Wang, X., Wekerle, C., Danilov, S., Jung, T., Koldunov, N., et al. (2019). Ocean heat transport into the Barents Sea: Distinct controls on the upward trend and interannual variability. *Geophysical Research Letters*, *46*(22), 13180–13190. https://doi.org/10.1029/2019gl083837

Wang, Q., Wekerle, C., Danilov, S., Wang, X., & Jung, T. (2018). A 4.5 km resolution Arctic Ocean simulation with the global multi-resolution model FESOM 1.4. *Geoscientific Model Development*, *11*(4), 1229–1255. https://doi.org/10.5194/gmd-11-1229-2018

Wang, Q., Wekerle, C., Wang, X., Danilov, S., Koldunov, N., Sein, D., et al. (2020). Intensification of the Atlantic Water supply to the Arctic Ocean through Fram Strait induced by Arctic sea ice decline. *Geophysical Research Letters*, *47*(3), e2019GL086682. https://doi.org/10.1029/2019gl086682

Woodgate, R. A., Aagaard, K., Muench, R. D., Gunn, J., Björk, G., Rudels, B., et al. (2001). The Arctic Ocean boundary current along the Eurasian slope and the adjacent Lomonosov Ridge: Water mass properties, transports and transformations from moored instruments. *Deep Sea Research Part I: Oceanographic Research Papers*, *48*(8), 1757–1792. https://doi.org/10.1016/s0967-0637(00)00091-1

Zhang, J., & Steele, M. (2007). Effect of vertical mixing on the Atlantic Water layer circulation in the Arctic Ocean. *Journal of Geophysical Research*, *112*(C4). https://doi.org/10.1029/2006jc003732